Metasurface-based scalar vortex phase mask in pursuit of 1e-10 contrast

Lorenzo König[a], Skyler Palatnick[b], Niyati Desai[c], Olivier Absil[a], Maxwell Millar-Blanchaer[b], and Dimitri Mawet[c,d]

[a]STAR Institute, Université de Liège, Allée du Six Août 19c, 4000 Liège, Belgium
[b]Department of Physics, University of California Santa Barbara, CA, USA
[c]Department of Astronomy, California Institute of Technology, CA, USA
[d]Jet Propulsion Laboratory, California Institute of Technology, CA, USA

ABSTRACT

Imaging Earth-like planets around Sun-like stars has become one of the main science drivers for future space telescope missions. High-contrast imaging using a vortex coronagraph has proven to be a promising approach for achieving this goal. However, at the huge contrast levels required for future space-based telescopes the vectorial nature of the well-established vector vortex phase mask becomes a limiting factor, since it imprints phase ramps of opposite signs on the two circular polarizations. An alternative polarization-independent approach is using a scalar vortex phase mask, which affects both polarizations in the same way. The achromatic performance of scalar vortex phase masks for space-based applications has still to be improved, though. Metasurfaces provide a promising approach to implement a scalar vortex phase mask with relatively simple fabrication techniques. Their demonstrated ability to implement broadband phase and amplitude masks makes them a prime candidate for achieving achromatic performance in pursuit of the 10^{-10} contrast limit required by NASA's Habitable Worlds Observatory. We present a metasurface-based design of a scalar vortex phase mask providing a helical phase ramp across a large bandwidth. We first use rigorous coupled-wave analysis to create a library of square metasurface building blocks (nanoposts) and choose an optimal set of nanopost sizes providing broadband 2π phase coverage at a given nanopost height. We then arrange the nanoposts in a design providing a helical phase ramp and propagate the phase and transmission provided by the mask through a wavefront propagation software to obtain contrast curves at several wavelengths. Finally we apply electric field conjugation to dig a half-sided dark hole from 3-10 λ/D reaching 3.7×10^{-9} contrast in 20 % bandwidth.

Keywords: Scalar vortex coronagraph, metasurfaces, diamond, exoplanet, design optimization

1. INTRODUCTION

The direct imaging goals for the Habitable Worlds Observatory (HWO) require a coronagraph that achieves a contrast of 10^{-10} at its inner working angle for a 20 % bandwidth. Both HabEx[1] and LUVOIR-B[2] feature a vector vortex coronagraph of topological charge 6 as the most suitable technology for starlight suppression, providing an inner working angle of 2.5 λ/D. Using wavefront control, and a polarizer-analyzer setup to remove polarization leakage, contrast values on the order of 2×10^{-9} have been demonstrated in lab for a bandwidth of 10 % using a vector vortex phase mask based on liquid crystal polymers.[3] However, differential polarization aberrations become difficult to control at such high contrasts, requiring careful wavefront control in both polarizations independently. This is challenging to achieve with a single or even multiple deformable mirrors because the vector vortex coronagraph is polarization-sensitive and imprints phase ramps of opposite signs on the two polarization states, requiring the polarizations to be split. This results in considerably more complex instrumental designs basically doubling the number of optics or eliminating half of the total throughput per channel. A polarization-independent (scalar) vortex coronagraph circumvents this issue since it imprints the same phase ramp regardless of polarization and is therefore an interesting alternative to the well established concept of the vector vortex coronagraph.

Scalar vortex coronagraphs using longitudinal phase delays have been shown to yield performance on the order of 10^{-8} in narrowband, and 2×10^{-7} across 10 % bandwidth, showing encouraging results so far.[4] Stacking

several layers of dielectrics is one possible solution to increase broadband performance but usually results in bulky components which are not suitable for use in the focal plane.[5,6]

The achromatic performance of scalar vortex phase mask designs remains a challenging goal. Compared to existing scalar vortex phase mask technologies based on the longitudinal phase delay of different dielectrics, a metasurface framework benefits from a better broadband performance within a single layer. This is due to the different metasurface topologies which introduce new degrees of freedom by changing the shape of their constituent building blocks. As a result, metasurfaces are a promising approach to increase the broadband performance of the scalar vortex coronagraph, which can be implemented with relatively simple and well established fabrication techniques. However, to date no study of a metasurface-based scalar vortex coronagraph for high contrast imaging applications has been reported.

Metasurfaces are thin structures consisting of subwavelength building blocks conveniently arranged to create a specific phase and amplitude response to an incoming beam. Recent developments have shown that metasurfaces can be engineered to provide precise 2π phase coverage and high throughput across large bandwidths.[7–9] This makes them a prime candidate for achromatic high-performance coronagraphs. Several applications of metasurfaces generating vortex beams have been reported[10–12] and recently significant progress has been made in making metasurface components achromatic across large bandwidths.[13–15] Polarization-independent metasurfaces consisting of circular or square nanoposts (more generally axially symmetric metasurfaces in both orthogonal axes) are of particular interest because they do not require polarization splitting, which is limiting the current vector vortex coronagraphs using subwavelength gratings or liquid crystal polymers. Combining a polarization-independent metasurface framework with the design of scalar vortex phase masks therefore greatly increases our ability to make the scalar vortex coronagraph achromatic and ready for the needs of future space telescope missions.

In Section 2 we introduce a metasurface framework based on square nanoblocks capable of providing full 2π phase coverage and high transmission at the same time. In Section 3 we optimize the performance of this framework for the application across 20 % bandwidth and propose a scalar vortex phase mask design for application in the infrared. Due to the scale-invariance of the problem, the results can be properly scaled for use in the visible wavelength range. In Section 4 we simulate the expected performance in a coronagraphic setup and outline the potential of wavefront control algorithms when applied to this design. Section 5 concludes this work and outlines the next steps towards a first prototype.

2. METASURFACE DESIGN FOR SCALAR VORTEX PHASE MASK

The design process of scalar vortex phase masks starts with the identification of a promising metasurface framework. Here, two similar frameworks are considered: circular nanoposts and square nanoblocks. These are the simplest shapes for a polarization-independent metasurface framework, and both can easily be arranged in a cartesian pixelization grid to sample the full phase mask. More complicated shapes can be envisaged, like hexagonal nanoposts on a hexagonal grid,[16] designs with varying spacing between the blocks[11] or shapes with holes or crosses,[17,18] introducing more degrees of freedom which could further improve broadband performance in the future. For an exploration of more complex metasurface patterns including multi-shape designs with varying spacing we refer to Ref. 19 in these proceedings.

To assess the phase and transmission properties of a metasurface framework, a series of RCWA simulations are performed. Using RCWA implies using a periodic and infinite pattern of metasurface building blocks. Locally, these conditions are fulfilled when a metasurface block is surrounded by other blocks of similar geometrical parameters. This is the case for most parts of the phase masks considered in this chapter, except at the 2π phase jumps and the central singularity.

The phase and transmission response of a periodic array of circular diamond nanoposts and square diamond nanoblocks etched into a diamond substrate is shown in Figure 1 for an exemplary metasurface height of 9.5 µm and a periodicity of 1.4 µm (for application in the astronomical L-band, 3.4-4.2 µm). The choice of a pattern etched into a single diamond substrate has favorable properties in terms of robustness, durability, as well as thermal and mechanical stability. The RCWA simulation is carried out for different pillar sizes (x-axis) at a wavelength of 3.8 µm. The most important quantity to assess the metasurface framework is the phase coverage

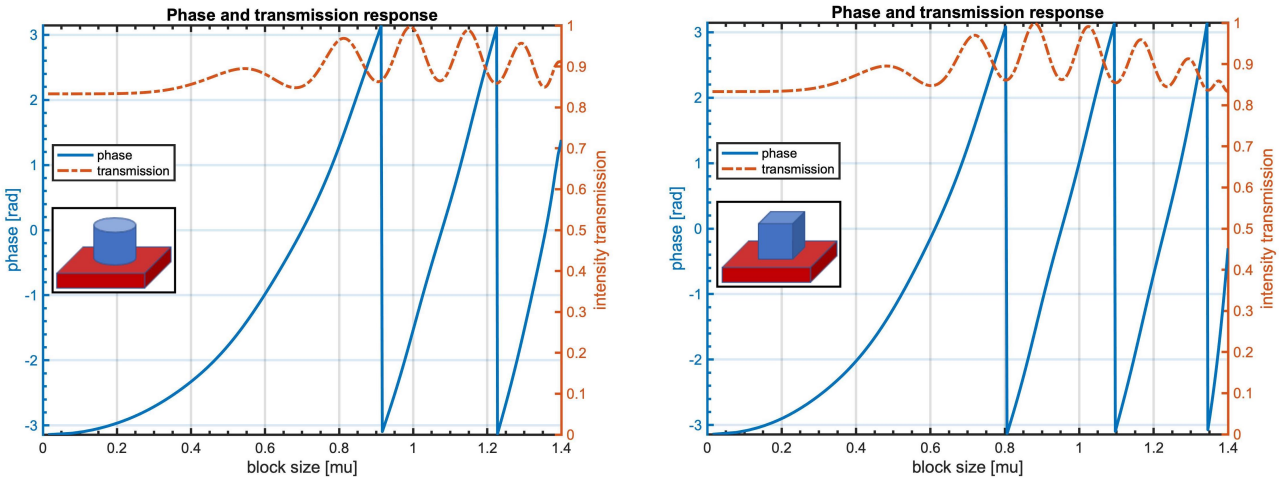

Figure 1. Phase (blue solid curve) and transmission (orange dashed curve) response of a circular diamond nanobloc (left) and square diamond nanoblock (right) metasurface framework at fixed height of 9.5 µm calculated with RCWA for $\lambda = 3.8\,\mu\text{m}$.

of 2π needed to imprint a helical phase ramp. The varying phase pattern of a vortex phase mask is achieved by spatially varying the optical path length across the mask. This is achieved by locally changing the effective refractive index, which itself depends on the local filling factor of the metasurface design. The achievable phase coverage increases with increasing metasurface height and therefore a certain minimum height is needed to provide full 2π phase coverage.

Compared to the circular nanoposts, the phase curves for square nanoblocks are steeper, meaning that 2π phase coverage is achieved with a smaller range of block sizes. This is favorable for manufacturing of these components, since large variations of the filling factor make manufacturing processes based on plasma etching challenging because of the microloading effect,[20] resulting in uneven etch depth. This is due to the varying size of the gaps in the design (between the nanoblocks) resulting in varying etch rate across the mask. Furthermore, a metasurface design using a smaller range of block sizes results in neighboring metasurface blocks being more similar to each other, which reduces the errors due to the pixelization grid in regions of fast spatial phase variations, like at the central singularity of the vortex phase ramp. Due to its advantages over the circular nanopost framework, the square nanoblock framework is chosen for the first scalar phase mask designs presented here. However, a circular nanopost metasurface framework might still be a valid option for other applications of phase masks, which depend in a different way on the phase and transmission than the vortex.

Another important quality of a metasurface framework for vortex phase masks is the uniformity of the transmission. A perfect vortex phase mask is a pure phase mask with uniform transmission. Therefore, a non-uniform transmission pattern arising from a non-uniform metasurface pattern has to be reasonably small. Typically, the 20 % transmission variation encountered in the metasurface frameworks considered in this chapter results in a peak-to-peak leakage term of the order of 10^{-6}, which is comparable to the chromatic phase error and therefore acceptable for the first scalar vortex phase masks discussed here. It is interesting to note that a non-zero sidewall angle (non-vertical height profile of the nanoposts) has an anti-reflective effect[21] and therefore results in smaller transmission variations. A design featuring slightly slanted sidewalls is therefore more favorable in terms of transmission uniformity, at the expense of a shallower phase curve requiring a larger range of block sizes to reach 2π phase coverage. On the other side, slanted sidewalls reduce the range of achievable filling factors for a design, since the sidewalls might touch at the bottom of small gaps in the design, which leads to merging blocks in those regions of the mask. Overall, the full 2π phase coverage is found to be more important to reach high contrasts than a uniform transmission, and therefore designs featuring vertical sidewalls will be preferred in this study. Moreover, varying transmission of the phase mask could be tackled by a grayscale pattern on the backside of the phase mask implemented in a similar way as amplitude apodizers. For manufacturing perspectives

however, vertical sidewalls are challenging to achieve and the performance of designs featuring slanted sidewalls needs to be estimated when envisaging manufacturing of a prototype.

3. OPTIMIZING FOR BROADBAND PERFORMANCE

While achromatic metasurface implementations in the literature focus mostly on the absolute phase response as used in metalenses,[22,23] there is no need to do so for vortex phase masks. The important metric for a vortex phase mask is to obtain the phase ramp corresponding to the topological charge of the vortex. For scalar vortices made of a helical shaped dielectric mask, the phase is highly chromatic. The key property of metasurfaces is that while the phase induced by the metasurface itself might be chromatic, the phase difference $\Delta\phi$ acquired along a closed path around the optical axis of the vortex phase mask can be engineered to be less chromatic across a certain bandwidth by optimizing the size of the metasurface building blocks. This is illustrated in Figure 2, which shows the effective refractive index n_{eff} along with the chromatic phase response for a square nanoblock framework at several wavelengths. While n_{eff} is chromatic, the phase difference $\Delta\phi$ is relatively achromatic across the 20 % bandwidth considered here.

After finding a metasurface framework providing 2π phase coverage across 20 % bandwidth, a scalar vortex design is produced using this framework. Here, we will focus on a charge-6 scalar vortex phase mask, as specified by the HabEx and LUVOIR mission concepts. This topological charge is small enough to provide relatively small inner working angle ($2.5\,\lambda/\text{D}$) and large enough to be resilient to the lowest order aberrations.

For the implementation of a scalar vortex with the present metasurface framework, a sawtooth vortex design featuring six 2π phase jumps is chosen. This choice is motivated by the limited phase coverage that can be achieved with a nanopost framework. The sawtooth design needs only 2π phase coverage, while a classical vortex needs $6 \cdot 2\pi = 12\pi$ coverage. Since the maximal height coverage of a nanopost framework is limited by the height of the nanoposts, the sawtooth design topology is chosen for a first nanopost scalar vortex phase mask design. Furthermore, the height and the variation of the block size across the mask has to be kept reasonably small to keep the design within reach for current manufacturing techniques.

Figure 3 shows a design for a sawtooth vortex of topological charge 6 using a nanoblock framework. The design shown is a closeup of the central part of the mask including the phase singularity. It is clearly visible that at increasing distance from the center the pattern becomes locally periodic, except at the 2π phase discontinuities. The design shown here is optimized for the astronomical L-band (3.4-4.1 µm) but due to the scale invariance of the problem the results can be applied to other wavelength bands, such as the visible range. However, due to the subwavelength condition, designs optimized for shorter wavelengths feature smaller building blocks and are therefore more challenging to manufacture. In addition, the design shown here is not optimal for manufacturing because of the very small distance between some of the blocks. Taking into account manufacturing constraints may lead to a slightly smaller width for all nanoblocks and slightly reduced performance.

4. CORONAGRAPHIC PERFORMANCE SIMULATIONS

After obtaining the near field response of the phase masks in the focal plane with RCWA, the performance in a coronagraphic system has to be evaluated. Here, the Airy pattern of a circular pupil is modulated with the near field response obtained with RCWA, and propagated to the subsequent pupil plane where a slightly undersized Lyot stop (90 %) is used to block the light diffracted outside the pupil, and further to the final focal plane producing the coronagraphic image. The Matrix Fourier Transform algorithm implemented in FALCO[24] is used to obtain the focal plane image.

Figure 4 shows the contrast curves of the nanoblock scalar vortex design at different wavelengths as well as the average contrast in a region from 3 to $10\,\lambda/\text{D}$. The nanopost design outperforms the theoretical vortex shown for comparison because of its optimization for a broad band. At the same time, at the central wavelength it performs significantly worse than the theoretical vortex. This is because while at the central wavelength both theoretical and nanopost vortex have the same perfect phase ramp, the nanopost framework suffers from varying transmission limiting the achievable contrast.

After obtaining the raw contrast, the performance in the scoring region between 3 and $10\,\lambda/\text{D}$ can be increased by using wavefront control algorithms and a deformable mirror to dig a dark hole in the coronagraphic image.

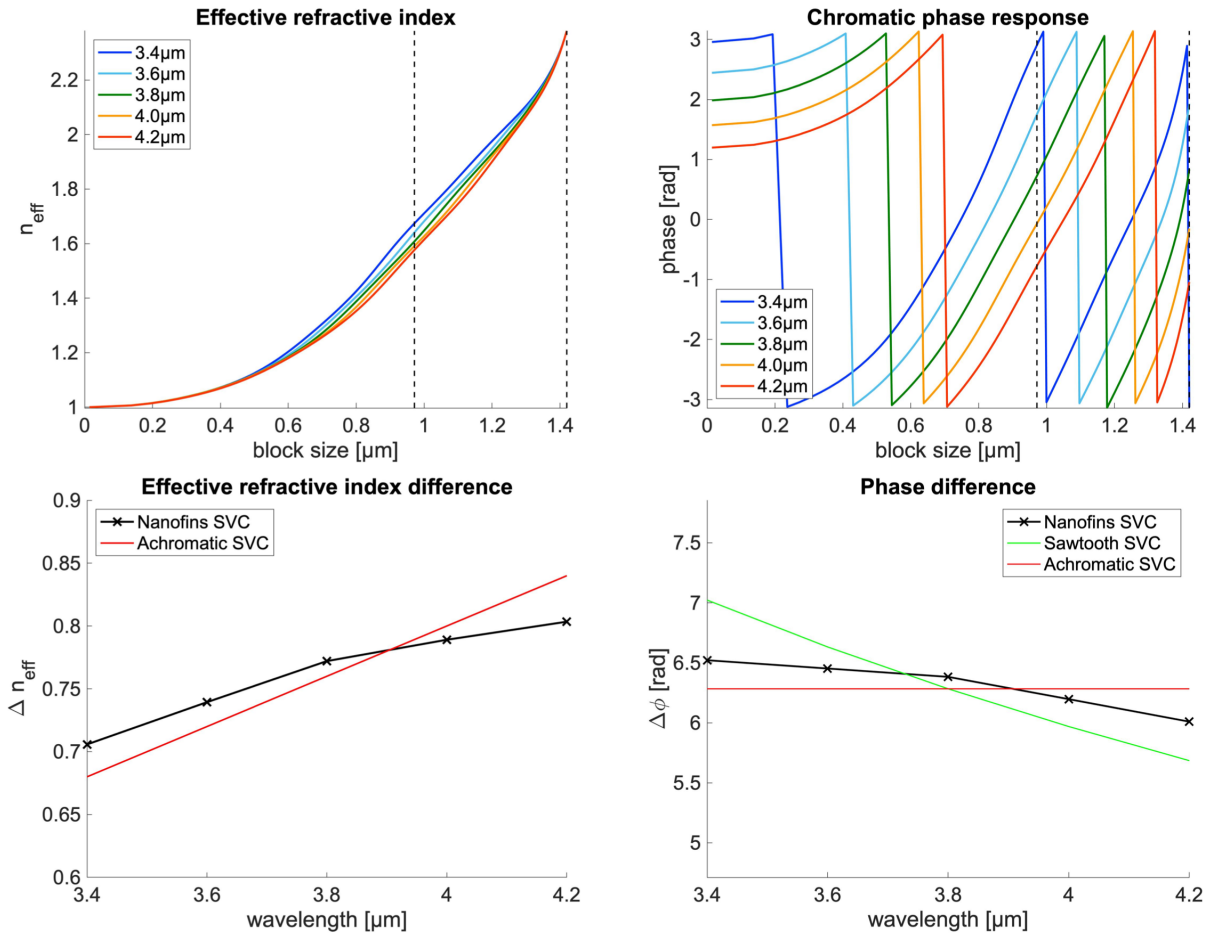

Figure 2. Chromaticity of a metasurface framework consisting of square nanoblocks. Top: Effective refractive index (left) and phase response (right). A metasurface framework consisting of square nanoblocks of relatively shallow height (5 µm) is chosen to illustrate the chromatic behavior of the effective refractive index n_{eff} (a larger height would feature steeper phase curves reducing the readability of the right graph). The optimal region providing broadband 2π phase coverage is highlighted with dashed black lines. Bottom: Effective refractive index difference Δn_{eff} (left) and phase difference $\Delta\phi$ (right) at the 2π phase discontinuities. While n_{eff} itself is chromatic, the acquired phase difference $\Delta\phi$ is relatively achromatic because the linear dependency of Δn_{eff} compensates for the $1/\lambda$ dependency of the phase difference. The achromatic vortex case is shown as red line, and the curve for a sawtooth scalar vortex (with six 2π phase jumps) made from a helical shaped dielectric mask is shown as green line.

Here, electric field conjugation (EFC)[25] is used to dig a dark hole with FALCO in a 178° dark hole between 3 and 10 λ/D. The resulting focal plane image is shown in Figure 5 along with the associated surface profile of the deformable mirror. Using EFC, the average contrast in the scoring region is 3.70×10^{-9} in 20 % bandwidth, which represents a moderate improvement by a factor of 3 compared to the raw contrast of 1.24×10^{-8}. The contrast values presented here are promising, but still far from the 10^{-10} goal. However, the use of more complex metasurface topologies combined with an optimized material choice could reach the required contrast.

5. CONCLUSION

A scalar metasurface framework using polarization independent symmetric building blocks was investigated for the implementation of scalar vortex phase masks. The study of square nanoblocks led to the design of a scalar vortex phase mask increasing the contrast by two orders of magnitude compared to a classical sawtooth scalar

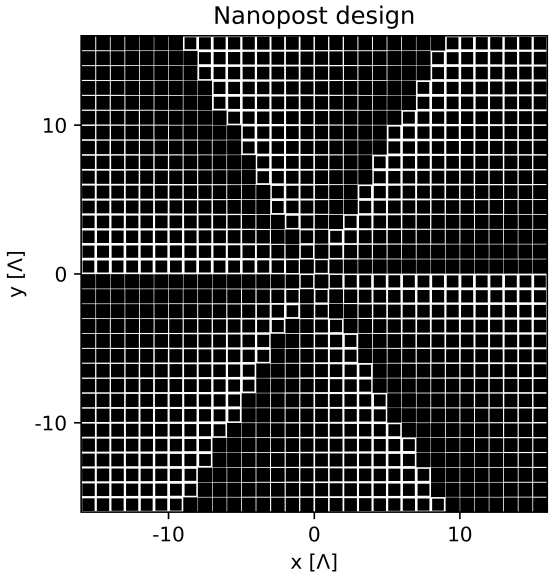

Figure 3. Square nanoblock design for a charge-6 scalar vortex phase mask.

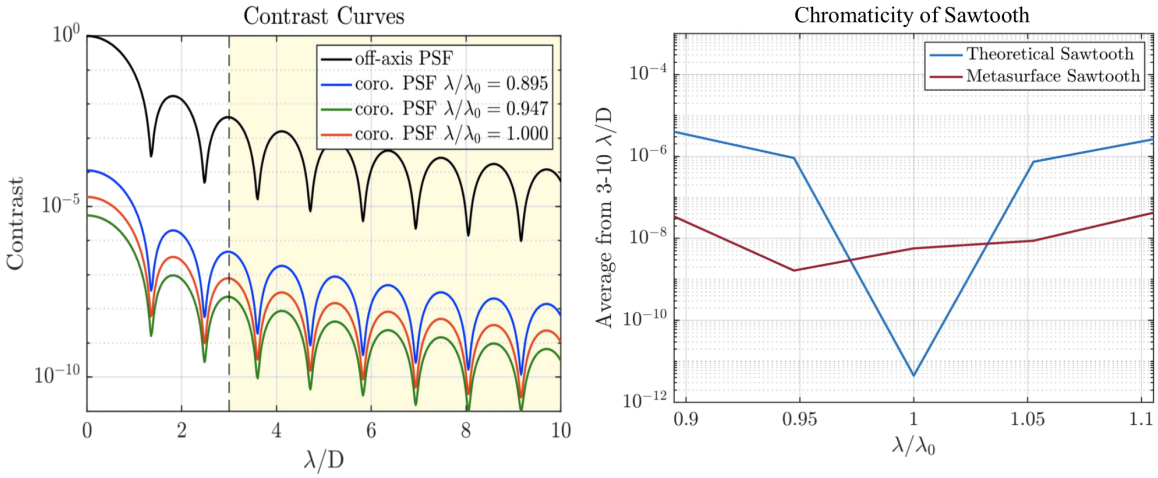

Figure 4. Contrast curves for a nanopost sawtooth vortex computed with FALCO at several wavelengths (left). Only three wavelengths are shown for the sake of clarity. The region of interest (3-10 λ/D) is highlighted (yellow), and used to obtain the averaged contrast shown in the second graph (right).

vortex phase mask. This technology is potentially applicable to future space telescope missions, which need contrasts on the order of 10^{-10} at the inner working angle of the coronagraph. Optimizing the two-dimensional metasurface framework for achromatic performance led to contrasts of 3.7×10^{-9} using a wavefront control algorithm, pushing the limits towards the requirements of future space telescopes tailored for imaging Earth-like planets around Sun-like stars. Although these preliminary results are still a factor 30 short of the 10^{-10} goal for HWO, this gap might be addressed with more complex designs featuring multiple shapes and variable period as described in Ref. 19 in these proceedings.

The manufacturing of a first prototype is an important next step in the development of two-dimensional metasurface implementations of vortex phase masks. It is therefore mandatory to advance the manufacturing capabilities in order to overcome the challenges expected with these designs, notably the high aspect ratio and the varying grating parameters across the mask. In addition, this involves the consideration of different materials

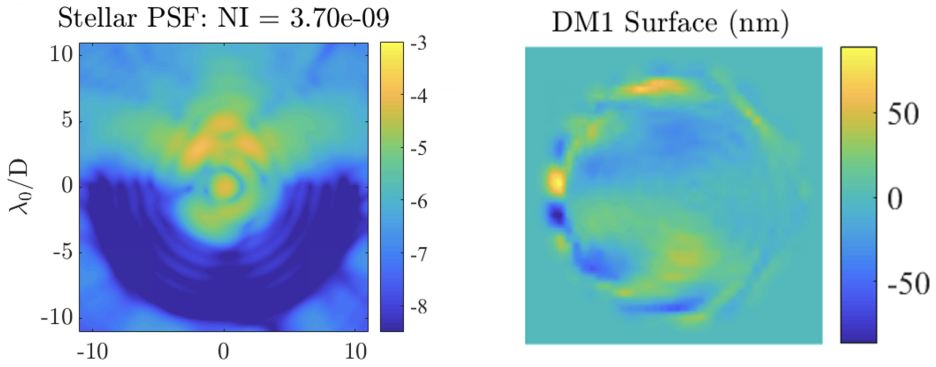

Figure 5. Dark hole obtained with EFC applied to a nanopost sawtooth vortex design (left) and respective surface profile of the deformable mirror (right). The scoring region is a circular region between 3 and 10 λ/D spanning 178° in the focal plane and optimized for 20 % bandwidth.

for a prototype and choosing the most promising manufacturing approach, depending on the wavelength of the application, the desired chromatic performance as well as the feasibility of the manufacturing process to provide a high-performance component. Moreover, it is important to accurately characterize the phase response of a manufactured component to understand the limitations of the simulations and the manufacturing process, as well as the manufacturing uncertainties and how they impact the performance of the component. Several iterations adapting the design process to the manufacturing constraints will be needed before obtaining a high-performance component.

ACKNOWLEDGMENTS

L.K. and O.A. acknowledge funding from the European Research Council (ERC) under the European Union's Horizon 2020 research and innovation programme (grant agreement No 819155).

REFERENCES

[1] Gaudi, B. S., Seager, S., Mennesson, B., Kiessling, A., Warfield, K., Cahoy, K., Clarke, J. T., Domagal-Goldman, S., Feinberg, L., Guyon, O., et al., "The habitable exoplanet observatory (habex) mission concept study final report," *arXiv preprint* , arXiv:2001.06683 (2020).

[2] The LUVOIR Team, "The luvoir mission concept study final report," *arXiv preprint* , arXiv:1912.06219 (2019).

[3] Ruane, G., Riggs, A. E., Serabyn, E., Baxter, W., Mejia Prada, C., Mawet, D., Noyes, M., Poon, P. K., and Tabiryan, N., "Broadband vector vortex coronagraph testing at nasa's high contrast imaging testbed facility," in [*Space Telescopes and Instrumentation 2022: Optical, Infrared, and Millimeter Wave*], *Proceedings of the SPIE* **12180**, 1218024, SPIE (2022).

[4] Desai, N., Ruane, G., Llop-Sayson, J., Betrou-Cantou, A., Potier, A., Riggs, A. E., Serabyn, E., and Mawet, D., "Laboratory demonstration of the wrapped staircase scalar vortex coronagraph," *Journal of Astronomical Telescopes, Instruments, and Systems* **9**(2), 025001 (2023).

[5] Swartzlander Jr, G. A., "Achromatic optical vortex lens," *Optics Letters* **31**(13), 2042–2044 (2006).

[6] Ruane, G., Mawet, D., Riggs, A. E., and Serabyn, E., "Scalar vortex coronagraph mask design and predicted performance," in [*Techniques and Instrumentation for Detection of Exoplanets IX*], *Proceedings of the SPIE* **11117**, 454–469, SPIE (2019).

[7] Yu, N. and Capasso, F., "Flat optics with designer metasurfaces," *Nature Materials* **13**(2), 139–150 (2014).

[8] Kruk, S., Ferreira, F., Mac Suibhne, N., Tsekrekos, C., Kravchenko, I., Ellis, A., Neshev, D., Turitsyn, S., and Kivshar, Y., "Transparent dielectric metasurfaces for spatial mode multiplexing," *Laser & Photonics Reviews* **12**(8), 1800031 (2018).

[9] Khorasaninejad, M., Chen, W. T., Devlin, R. C., Oh, J., Zhu, A. Y., and Capasso, F., "Metalenses at visible wavelengths: Diffraction-limited focusing and subwavelength resolution imaging," *Science* **352**(6290), 1190–1194 (2016).

[10] Devlin, R. C., Ambrosio, A., Wintz, D., Oscurato, S. L., Zhu, A. Y., Khorasaninejad, M., Oh, J., Maddalena, P., and Capasso, F., "Spin-to-orbital angular momentum conversion in dielectric metasurfaces," *Opt. Express* **25**(1), 377–393 (2017).

[11] Chong, K. E., Staude, I., James, A., Dominguez, J., Liu, S., Campione, S., Subramania, G. S., Luk, T. S., Decker, M., Neshev, D. N., Brener, I., and Kivshar, Y. S., "Polarization-independent silicon metadevices for efficient optical wavefront control," *Nano Letters* **15**(8), 5369–5374 (2015).

[12] Shalaev, M. I., Sun, J., Tsukernik, A., Pandey, A., Nikolskiy, K., and Litchinitser, N. M., "High-efficiency all-dielectric metasurfaces for ultracompact beam manipulation in transmission mode," *Nano Letters* **15**(9), 6261–6266 (2015).

[13] Heiden, J. T. and Jang, M. S., "Design framework for polarization-insensitive multifunctional achromatic metalenses," *Nanophotonics* **11**(3), 583–591 (2022).

[14] Sun, T., Hu, J., Ma, S., Xu, F., and Wang, C., "Polarization-insensitive achromatic metalens based on computational wavefront coding," *Optics Express* **29**(20), 31902–31914 (2021).

[15] Li, X. and Fan, Z., "Controlling dispersion characteristic of focused vortex beam generation," *Photonics* **9**(3), 179, MDPI (2022).

[16] Arbabi, A., Horie, Y., Bagheri, M., and Faraon, A., "Dielectric metasurfaces for complete control of phase and polarization with subwavelength spatial resolution and high transmission," *Nature nanotechnology* **10**(11), 937–943 (2015).

[17] Shrestha, S., Overvig, A. C., Lu, M., Stein, A., and Yu, N., "Broadband achromatic dielectric metalenses," *Light: Science & Applications* **7**(1), 85 (2018).

[18] Chen, W. T., Park, J.-S., Marchioni, J., Millay, S., Yousef, K. M., and Capasso, F., "Dispersion-engineered metasurfaces reaching broadband 90% relative diffraction efficiency," *Nature Communications* **14**(1), 2544 (2023).

[19] Palatnick, S., König, L., Millar-Blanchaer, M., Wallace, J., Absil, O., Mawet, D., Desai, N., Echeverri, D., John, D., and Schuller, J., "Metasurfaces in exoplanet direct imaging systems: from principles to fabrication," in [*Techniques and Instrumentation for Detection of Exoplanets XI*], *Proceedings of the SPIE* , SPIE (2023).

[20] Hedlund, C., Blom, H.-O., and Berg, S., "Microloading effect in reactive ion etching," *Journal of Vacuum Science & Technology A: Vacuum, Surfaces, and Films* **12**(4), 1962–1965 (1994).

[21] Forsberg, P. and Karlsson, M., "Inclined surfaces in diamond: broadband antireflective structures and coupling light through waveguides," *Optics Express* **21**(3), 2693–2700 (2013).

[22] Chung, H. and Miller, O. D., "High-na achromatic metalenses by inverse design," *Optics Express* **28**(5), 6945–6965 (2020).

[23] Chen, W. T., Zhu, A. Y., and Capasso, F., "Flat optics with dispersion-engineered metasurfaces," *Nature Reviews Materials* **5**(8), 604–620 (2020).

[24] Riggs, A. E., Ruane, G., Sidick, E., Coker, C., Kern, B. D., and Shaklan, S. B., "Fast linearized coronagraph optimizer (falco) i: a software toolbox for rapid coronagraphic design and wavefront correction," in [*Space Telescopes and Instrumentation 2018: Optical, Infrared, and Millimeter Wave*], *Proceedings of the SPIE* **10698**, 878–888, SPIE (2018).

[25] Give'on, A., Kern, B., Shaklan, S., Moody, D. C., and Pueyo, L., "Electric field conjugation-a broadband wavefront correction algorithm for high-contrast imaging systems," in [*American Astronomical Society Meeting Abstracts*], *American Astronomical Society Meeting Abstracts* **211**, 135–20 (2007).